

## RESEARCH LETTER

10.1002/2017GL073128

## Key Points:

- Cloud base charge is sensed remotely using its effect on the surface electric field
- About 75% of layer clouds observed have appreciably negatively charged cloud bases

## Supporting Information:

- Supporting Information S1

## Correspondence to:

K. A. Nicoll,  
k.a.nicoll@reading.ac.uk

## Citation:

Harrison, R. G., K. A. Nicoll, and K. L. Aplin (2017), Evaluating stratiform cloud base charge remotely, *Geophys. Res. Lett.*, 44, 6407–6412, doi:10.1002/2017GL073128.

Received 17 FEB 2017

Accepted 1 JUN 2017

Accepted article online 5 JUN 2017

Published online 17 JUN 2017

## Evaluating stratiform cloud base charge remotely

R. Giles Harrison<sup>1</sup> , Keri A. Nicoll<sup>1,2</sup> , and Karen L. Aplin<sup>3</sup> 
<sup>1</sup>Department of Meteorology, University of Reading, Reading, UK, <sup>2</sup>Department of Electronic and Electrical Engineering, University of Bath, Bath, UK, <sup>3</sup>Department of Physics, University of Oxford, Oxford, UK

**Abstract** Stratiform clouds acquire charge at their upper and lower horizontal boundaries due to vertical current flow in the global electric circuit. Cloud charge is expected to influence microphysical processes, but understanding is restricted by the infrequent in situ measurements available. For stratiform cloud bases below 1 km in altitude, the cloud base charge modifies the surface electric field beneath, allowing a new method of remote determination. Combining continuous cloud height data during 2015–2016 from a laser ceilometer with electric field mill data, cloud base charge is derived using a horizontal charged disk model. The median daily cloud base charge density found was  $-0.86 \text{ nC m}^{-2}$  from 43 days' data. This is consistent with a uniformly charged region  $\sim 40 \text{ m}$  thick at the cloud base, now confirming that negative cloud base charge is a common feature of terrestrial layer clouds. This technique can also be applied to planetary atmospheres and volcanic plumes.

**Plain Language Summary** The idea that clouds in the atmosphere can charge electrically has been appreciated since the time of Benjamin Franklin, but it is less widely recognized that it is not just thunderclouds which contain electric charge. For example, water droplets in simple layer clouds, that are abundant and often responsible for an overcast day, carry electric charges. The droplet charging arises at the upper and lower edges of the layer cloud. This occurs because the small droplets at the edges draw charge from the air outside the cloud. Understanding how strongly layer clouds charge is important in evaluating electrical effects on the development of such clouds, for example, how thick the cloud becomes and whether it generates rain. Previously, cloud charge measurement has required direct measurements within the cloud using weather balloons or aircraft. This work has monitored the lower cloud charge continuously using instruments placed at the surface beneath. From measurements made over 2 years, the cloud base charge is negative in the majority of cases. This confirms that charging of layer clouds is not a random process but instead arises from fundamental aspects of the atmosphere's structure.

## 1. Introduction

Stratiform clouds are the most abundant cloud type, typically covering 30% of the globe, and their radiative properties have a significant effect on climate [e.g., Klein and Hartmann, 1993; Wood, 2015]. One key property, which is relatively poorly appreciated, is that these layer clouds acquire charge at their upper and lower horizontal boundaries, from the global atmospheric electric circuit's vertical conduction current passing through the conductivity transition between clear and cloudy air [e.g., Zhou and Tinsley, 2007]. The cloud base charge depends on the local meteorological circumstances defining the cloud boundaries, the local ionization rate [e.g., Harrison et al., 2014], and the vertical conduction current density. Cloud charge is expected to affect cloud microphysics through droplet coalescence [Harrison et al., 2015] and droplet-aerosol scavenging [Tinsley et al., 2000]. However, little new information on non-thunderstorm cloud charging has been forthcoming since the pioneering measurements of the 1950s [e.g., Imyanitov and Chubarina, 1967; Jones et al., 1959], with some data now available from occasional in situ measurements at the cloud boundary [Nicoll and Harrison, 2010; Nicoll, 2012; Tsurudome et al., 2013]. Recently, balloon-borne instrumentation has established the presence of layer cloud edge charge at three locations over both hemispheres [Nicoll and Harrison, 2016]. Since the measurements to date have been restricted to airborne platforms, the abundance of charged cloud bases is not well known, which is important for evaluating the importance of charge in microphysical processes, and ultimately weather and climate. Here a new remote sensing technique is used to quantify the prevalence of cloud base charge continuously over 2 years at one midlatitude site, extending the previous findings from balloon soundings alone.

©2017. The Authors.

This is an open access article under the terms of the Creative Commons Attribution License, which permits use, distribution and reproduction in any medium, provided the original work is properly cited.

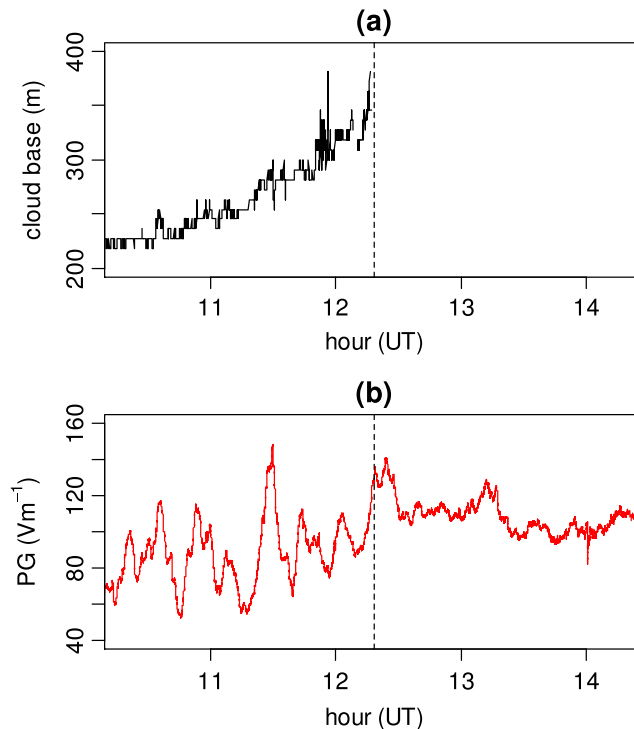


**Figure 1.** Variations in surface electric potential gradient (PG), before and after a low-level extensive stratiform cloud dissipated above Reading Observatory on 20 March 2015. Time series of measurements from (a) a Vaisala CL31 laser ceilometer determination of cloud base height (5 s samples) and (b) a JCI131 electric field mill (1 s samples) mounted at 3 m with its sensing aperture upward. The dashed line marks the time of the cloud dissipation.

Because a single balloon sounding only provides an instantaneous cloud edge charge measurement as the instruments pass through the lower cloud boundary, other techniques need to be investigated to provide continuous cloud base charge measurements. One approach is to consider the effect of the cloud base charge on the surface electric field ( $E_z$ ). This can sometimes be seen directly. Figure 1 shows an example of rapid samples of the cloud base height as determined by a laser ceilometer, with colocated samples of the vertical potential gradient, PG ( $F$  in equations), measured by an electric field mill, where, by convention,  $F = -E_z$ . These instruments, a JCI131 all weather field mill and a Vaisala CL31 ceilometer, were operated at the Reading University Atmospheric Observatory ([http://www.met.reading.ac.uk/observatorymain/Observatory\\_introduction.html](http://www.met.reading.ac.uk/observatorymain/Observatory_introduction.html)). The variability in PG decreased markedly in magnitude after the cloud dissipated, generating rapid but small fluctuations. Under the cloud, the typical time scales of the fluctuations were between 10 and 20 min. (This cloud layer was particularly keenly monitored as it obscured the partial solar eclipse earlier that day at around 0930 UT: the full meteorological and atmospheric electrical conditions for these circumstances at the site are described by Burt [2016] and Bennett [2016]).

A comparison of simultaneous colocated cloud base height and PG measurements during 2015 and 2016 at Reading is presented in Figure 2, for circumstances when the PG was positive but the cloud not strongly electrified (so could be assumed not to be mixed phase or convective). It is clear from this that there is a variation of PG with cloud base height when the cloud base is below about 800 m but that no strong effect on the PG exists when the cloud base is above 1000 m. (Cloud base heights below 100 m were excluded from this analysis as these are poorly determined by the ceilometer, and these values are usually also associated with fog, which considerably increases the PG through a near-surface reduction in the air conductivity.) The suppression in PG apparent from Figure 2b as the cloud base lowers is consistent with negative cloud base charge being brought closer to the surface. This does not preclude the existence of one or more additional charge layers above; however, surface PG measurements will be most strongly affected by the

The charge associated with the lower edge of a horizontally extensive layer cloud depends on the vertical gradient of conductivity across the cloud-air boundary and the vertical current flowing through the boundary. On solely electrostatic considerations, assuming steady state and no horizontal divergence of the current density  $J_c$ , the charge per unit volume  $\rho$  is

$$\begin{aligned}\rho &= -\epsilon_0 J_c \frac{d}{dz} \left( \frac{1}{\sigma_t} \right) \\ &= \epsilon_0 J_c \left( \frac{1}{\sigma_t^2} \right) \frac{d\sigma_t}{dz},\end{aligned}\quad (1)$$

where the total conductivity is  $\sigma_t$ ,  $z$  is height, and  $\epsilon_0$  is the permittivity of free space. Equation (1) shows that the charge density at the lower cloud boundary is negative (i.e., where  $\frac{d\sigma_t}{dz}$  is negative for  $z$  positive upward, as the conductivity decreases from the clear air beneath into the cloud above). From balloon soundings made through stratiform clouds in both hemispheres, Nicoll and Harrison [2016] reported a mean cloud base charge of  $-24 \text{ pC m}^{-3}$ .

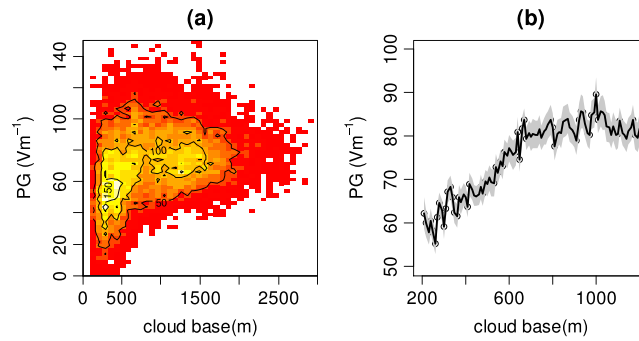


**Figure 2.** Cloud base height values plotted against surface potential gradient (PG), as 5 min averages obtained between 1 Jan 2015 and 31 Dec 2016, for positive PG values less than  $250 \text{ Vm}^{-1}$  and cloud base heights above 100 m. (a) Contoured histogram for the 91,867 available data values, with contours drawn to show the number of values in steps of 50, 100, and 150. (b) Mean PG (solid black line) calculated for the associated cloud base values binned into steps of 10 m, with 95% confidence limits on the mean shown by the grey bands.

tance. In evaluating the electric field beneath a cloud due to the cloud base charge, a finite radius charged disk provides a realistic description. Empirically, this approach is supported by the consistent charging of the stratiform cloud boundary, found on the regional scale by repeated measurements of the same cloud boundary [e.g., Nicoll and Harrison, 2016, Figure 3]. Practically, the cloud base disk charge can be sensed directly by an upward facing surface electric field mill, with geometry essentially described by a cone having its apex at the field mill position (see Figure S1 in the supporting information). A further important aspect of the finite disk model over point or line charge representations is that it allows the cloud base charge density to be calculated.

A cloud base disk charge of radius  $R$  and a charge density  $Q$  will enhance or reduce the clear-sky surface potential gradient  $F_0$ . The modified surface potential gradient  $F_s$  is given by

$$F_s = F_0 + \frac{Q}{2\epsilon_0} \left[ 1 - \frac{H}{(H^2 + R^2)^{1/2}} \right] \quad (2)$$

which is increased or reduced depending on whether  $Q$  is positive or negative, respectively. For a negative cloud base charge density  $Q$ , the variation of  $F_s$  with  $H$  indicated by equation (2) is consistent with the averaged variation seen in Figure 2: when the cloud base is high ( $H \gg R$ ) the second right-hand side term of equation (2) tends to zero and  $F_s \rightarrow F_0$ , whereas for a low cloud base ( $H \sim R$ ),  $F_s < F_0$ .

A charged disk representation implies a zone of homogenous charge. For such a uniformly charged disk, variations in the electric field beneath will only arise from displacement of the charged zone, such as that induced by the horizontal wind. The time scale  $\tau$  of associated electric field fluctuations would then be given by

$$\tau = \frac{R}{u}, \quad (3)$$

where  $u$  is the horizontal wind speed at the cloud base level and  $R$  is the disk radius.

### 3. Data Analysis

Equation (2) can be used to determine the cloud base charge density  $Q$  if all the other parameters are known or can be derived. For a colocated field mill and ceilometer beneath the same cloud, the surface potential

cloud base charge, which will also screen out charged layers above it. Measurement of multiple cloud charge zones will still require an in situ sounding, as the full vertical charge structure is likely to be complex [e.g., Tsurudome et al., 2013; Nicoll and Harrison, 2016].

## 2. Methodology

Associated with any charge is an electric field with magnitude proportional to the charge, and inversely proportional to the distance away from the charge at which it is determined. The geometry used to represent the charge (e.g., as a point, line, or disk) determines the form of the field variation with dis-

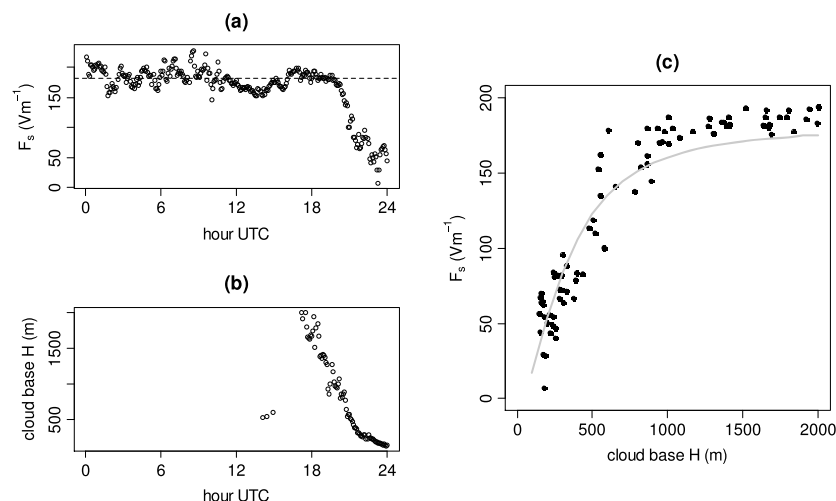


**Figure 3.** Time series of (a) surface potential gradient  $F_s$  and (b) cloud base height  $H$ , for 23 January 2015, using 5 min averages. In Figure 3a, the mean  $F_s$  ( $181 \text{ V m}^{-1}$ ) when  $1000 \text{ m} < H < 1500 \text{ m}$  is shown as the dashed horizontal line. (c) A plot of  $H$  against  $F_s$  with a fit under the assumption of a charged disk in the cloud base of radius  $R$  of charge density  $Q$ , for  $H > 100 \text{ m}$ . The fitted parameters are  $Q = -(3.6 \pm 2.3) \text{ nC m}^{-2}$  and  $R = (487 \pm 44) \text{ m}$ .

gradient  $F_s$  and cloud height  $H$  are obtained directly, but the equivalent effective radius of the charged disk  $R$  and the clear-sky surface potential gradient  $F_0$  are not known. However, Figure 2 indicates that for cloud bases at some distance from the surface, the surface PG becomes independent of the cloud base height. In this region of the parameter space the PG values are consistent with typical fair weather measurements at the site [Bennett and Harrison, 2007], and hence, this cloud-independent PG provides an estimate of  $F_0$ . The remaining two parameters,  $Q$  and  $R$ , can be found by a nonlinear fit of equation (2) to a set of measurements of  $F_s$  and  $H$ .

### 3.1. Single Day

This fitting approach is illustrated in Figure 3, which shows the time series across a day of (a)  $F_s$  and (b)  $H$ , during which a cloud forms in the last quarter of the day and its base steadily descends. The cloud-independent PG (which is regarded as  $F_0$ ) was also found, by averaging the  $F_s$  values when  $1000 \text{ m} < H < 1500 \text{ m}$ . Figure 3c shows a plot of  $F_s$  against  $H$ . This individual day's measurements, where the cloud base change is clearly identifiable, shows a similar response to the average of the 2 years of values in Figure 2b. Figure 3c includes a fit line made to equation (2) using the values of  $F_s$  against  $H$ , using the nonlinear least squares Gauss-Newton algorithm in the *R* statistical package [R Core Team, 2015]. This fitting algorithm is iterative and requires initial values, for which values of  $R = 500 \text{ m}$  and  $Q = 5 \text{ nC m}^{-2}$  were used, although the algorithm is not sensitive to the exact values of the initial guesses. The mean  $F_0$  value found from the cloud-independent region was also used as an input variable. The fit converged after 11 iterations to a tolerance of better than  $10^{-5}$ , with both fitting parameters statistically significant. Derived parameters were  $Q = -(3.6 \pm 2.3) \text{ nC m}^{-2}$  and  $R = (487 \pm 44) \text{ m}$ , where the uncertainty given is one standard error.

Clearly, this technique is limited by how well the cloud base can be defined by the ceilometer, and whether evaporation of charged drops (virga) occurs at appreciable distances beneath the observed cloud base.

### 3.2. Multiple Days

The agreement between the model and the data for a single day encouraged a similar analysis for all the  $F_s$  and  $H$  data available during 2015 and 2016. Fits to equation (2) for each day were sought using 5 min averages, for as many values as were available. To select circumstances more likely to be stratiform cloud conditions to which equation (1) applies, the cloud base heights were initially restricted to  $100 \text{ m} < H < 2000 \text{ m}$ . Even so, not all attempts to fit equation (2) converged, and of those that did, only a subset gave convincing fits. To select days with successful fits, a criterion was added that both the retrieved values for  $Q$  and  $R$  should be statistically significant (i.e.,  $p < 0.05$  in both cases). Statistical significance criteria are, however, essentially

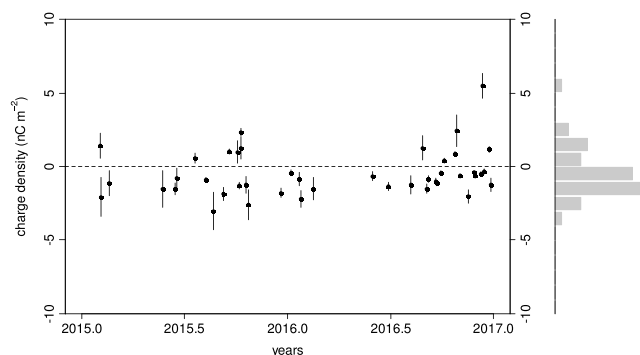


**Figure 4.** Daily cloud base charge density during 2015 and 2016, for dry days on which fitting the charged disk model to cloud base height and surface PG measurements gave a statistically significant ( $p < 0.05$ ) cloud base charge density and charged disk radius (43 days). Error bars show 95% confidence limits on the charge density derived from the fit.

to 861 m) and for  $Q$  the median was  $-0.86 \text{ nC m}^{-2}$  (IQR:  $-1.43 \text{ nC m}^{-2}$  to  $0.47 \text{ nC m}^{-2}$ ). The disk radius  $R$  is fairly narrowly constrained, indicating an approximate charge length scale of  $\sim 500 \text{ m}$  to which the field mill responds. From these estimates of  $R$  and assuming typical wind speeds at the cloud base of  $5$  to  $10 \text{ ms}^{-1}$ , equation (3) gives an associated fluctuation time scale in electric field of  $\tau \sim 100 \text{ s}$ . The observed fluctuations beneath cloud apparent in Figure 1 occur on much longer duration time scales ( $\sim 20 \text{ min}$ ), indicating charge homogeneity on length scales much greater than  $R$ .

Figure 4 presents the derived  $Q$  values as a time series, with an integral histogram. It is clear that the cloud base charge density is almost always negative (31 of 43 days), and for those cases which the charge density is positive, appreciable error bars are associated with the fit. Further investigation of the weather conditions at the site for the positive charge days suggest that many of these result from low-level fog substantially increasing the PG positively. Because of the variation in depth of different surface fog layers, these circumstances cannot be straightforwardly excluded from the data without jeopardizing genuinely fog-free fits in which the lower cloud bases strongly influence the results.

### 3.3. Effect of Cloud Duration

The days analyzed all had persistent cloud, but of different durations. The duration was calculated as the longest continuous period of available cloud base height determinations on a particular day. By comparing daily cloud duration with its derived base charge, it was found that a daily cloud duration of greater than 16 h (see Figure S2a) was required for the cloud base charge to reach its maximum magnitude and become independent of cloud duration. Using a Wilcoxon test (Figure S2b), the cloud base charge was significantly ( $p < 0.05$ ) nonzero for cloud durations longer than the median duration of 12.2 h. This minimum duration of cloud for a negative cloud base charge to be robustly established indicates a sustained cloud layer. This finding also supports the assumption that the observed modulation of surface PG is associated with persistent layer clouds, as frontal clouds typically vary over shorter time scales.

## 4. Discussion

Continuous measurements of cloud base charge provide key information for investigating the effects of charge on droplet formation and growth [Harrison *et al.*, 2015] and droplet-aerosol scavenging [Tinsley *et al.*, 2000]. The influence of cloud base charge on surface PG provides a basis on which to determine the cloud base charge remotely, using ceilometer and electric field mill data, without the need for in situ measurements.

669 complete days of data were available in 2015–2016. Of these days, there were 58 dry days on which clouds persisted for longer than 12.2 h (the median in Figure S2a), and valid fits (as defined in Figure 3c) were obtained on 43 days. This indicates that the technique was applicable on about three quarters of days likely to have sufficiently persistent stratiform clouds for charge to build up. From these measurements, the cloud

arbitrary, as any level of significance can be chosen, but applying the same requirements to all days' data offered some uniformity in the quality of the fits retained. A further criterion was that for each day considered, there should be no rainfall recorded. This was interpreted as daily rainfall of less than 0.2 mm at the site's tipping bucket rain gauge.

Following this selection approach, fits for  $Q$  and  $R$  from 43 dry days during 2015 and 2016 were retained for further analysis. For  $R$ , the median value was 663 m (interquartile range (IQR): 385 m

base charge was almost always negative, as expected from equation (1). The median cloud base charge on the assumption of a uniform disk charge density in the cloud base of  $-0.86 \text{ nC m}^{-2}$  should be compared with the instantaneous in situ measurements of charge per unit volume from balloon soundings of  $-24 \text{ pC m}^{-3}$  [Nicoll and Harrison, 2016]. Assuming that the lower cloud base represents a uniform disk of charge with  $-24 \text{ pC m}^{-3}$ , the thickness of the layer required would be about 40 m. This is consistent with the typical thickness of charge layers observed previously [Nicoll and Harrison, 2010, 2016] and indicates that charge at the base is a ubiquitous property of low-level layer clouds. Further work is needed to determine the microphysical effects of the charging and its potential role for the cloud's radiative properties and precipitation.

## 5. Conclusions

This work establishes for the first time by remote sensing that negative charge is prevalent in the bases of layer clouds, during 2 years of measurements over Reading, UK. This adds to in situ evidence of cloud base charge observed at two other sites near the poles [Nicoll and Harrison, 2016]. The new cloud charge sensing technique presented here has broader applications, from monitoring charged volcanic plumes [James et al., 1998] to other planets with stratiform-like clouds, such as Jupiter and Saturn [e.g., Showman and de Pater, 2005]. Evidence of similar electric field modulation, as the distance between a cloud and an electric field sensor changes, would allow the existence of a planetary global electric circuit [Aplin et al., 2008] to be inferred without the need for measurements of vertical current flow.

## Acknowledgments

K.A.N. acknowledges a NERC Independent Research Fellowship (NE/L011514/1). R. Brugge processed the Observatory measurements; data can be obtained from <http://www.met.rdg.ac.uk/observatorymain/>.

## References

- Aplin, K. L., R. G. Harrison, and M. J. Rycroft (2008), Investigating Earth's atmospheric electricity: A role model for planetary studies, *Space Sci. Rev.*, 137(1–4), 11–27, doi:10.1007/s11214-008-9372-x.
- Bennett, A. J. (2016), Effects of the March 2015 solar eclipse on near-surface atmospheric electricity, *Phil. Trans. R. Soc. London A*, 374(2077), 20150215.
- Bennett, A. J., and R. G. Harrison (2007), Atmospheric electricity in different weather conditions, *Weather*, 62(10), 277–283.
- Burt, S. (2016), Meteorological responses in the atmospheric boundary layer over southern England to the deep partial eclipse of 20 March 2015, *Phil. Trans. R. Soc. London A*, 374(2077), 20150214.
- Harrison, R. G., K. A. Nicoll, and K. L. Aplin (2014), Vertical profile measurements of lower troposphere ionisation, *J. Atmos. Sol. Terr. Phys.*, 119, 203–210, doi:10.1016/j.jastp.2014.08.006.
- Harrison, R. G., K. A. Nicoll, and M. H. P. Ambaum (2015), On the microphysical effects of observed cloud edge charging, *Q. J. R. Meteorol. Soc.*, 141, 2690–2699, doi:10.1002/qj.2554.
- Imyanitov, I. M., and E. V. Chubarina (1967), *Electricity of the Free Atmosphere*, Israel Program for Scientific Translations, Jerusalem.
- James, M. R., S. J. Lane, and J. S. Gilbert (1998), Volcanic plume monitoring using atmospheric electric potential gradients, *J. Geol. Soc.*, 155(4), 587–590.
- Jones, O. C., R. S. Maddever, and J. H. Sanders (1959), Radiosonde measurement of vertical electric field and polar conductivity, *J. Sci. Instrum.*, 36, 24–28.
- Klein, S. A., and D. L. Hartmann (1993), The seasonal cycle of low stratiform clouds, *J. Clim.*, 6(8), 1587–1606.
- Nicoll, K. A. (2012), Measurements of atmospheric electricity aloft, *Surv. Geophys.*, 33(5), 991–1057.
- Nicoll, K. A., and R. G. Harrison (2010), Experimental determination of layer cloud edge charging from cosmic ray ionisation, *Geophys. Res. Lett.*, 37, L13802, doi:10.1029/2010GL043605.
- Nicoll, K. A., and R. G. Harrison (2016), Stratiform cloud electrification: Comparison of theory with multiple in-cloud measurements, *Q. J. R. Meteorol. Soc.*, 142(700), 2679–2691.
- R Core Team (2015), *R: A Language and Environment for Statistical Computing*, R Foundation for Statistical Computing, Vienna, Austria. [Available at <http://www.R-project.org/>.]
- Showman, A. P., and I. de Pater (2005), Dynamical implications of Jupiter's tropospheric ammonia abundance, *Icarus*, 174(1), 192–204.
- Tinsley, B. A., R. P. Rohrbaugh, M. Hei, and K. V. Beard (2000), Effects of image charges on the scavenging of aerosol particles by cloud droplets and on droplet charging and possible ice nucleation processes, *J. Atmos. Sci.*, 57, 2118–21134.
- Tsurudome, C., et al. (2013), Measurement of the atmospheric electric field inside the nonthunderstorm clouds on 2012 BEXUS campaign, *J. Atmos. Electr.*, 33(2), 77–80.
- Wood, R. (2015), Stratus and stratocumulus, in *Encyclopedia of Atmospheric Sciences*, 2nd ed., vol. 2, edited by G. R. North, J. Pyle, and F. Zhang, pp. 196–200, Elsevier.
- Zhou, L., and B. A. Tinsley (2007), Production of space charge at the boundaries of layer clouds, *J. Geophys. Res.*, 112, D11203, doi:10.1029/2006JD007998.